Linear and nonlinear infrared signatures of local a-and 310-helical structures in alanine polypeptides

ARTICLE *in* THE JOURNAL OF CHEMICAL PHYSICS · FEBRUARY 2003

Impact Factor: 2.95 · DOI: 10.1063/1.1538243

4 AUTHORS, INCLUDING:

Shaul Mukamel
University of California, Irvine
852 PUBLICATIONS **23,706** CITATIONS

SEE PROFILE

Linear and nonlinear infrared signatures of local α- and 3_{10}-helical structures in alanine polypeptides

Andrew M. Moran, Seung-Min Park, Jens Dreyer, and Shaul Mukamel[a)]
Department of Chemistry, University of Rochester, Rochester, New York 14627-0216

(Received 22 October 2002; accepted 25 November 2002)

Vibrational exciton Hamiltonians for the amide I and amide A modes of both the α- and 3_{10}-helical conformations of a fifteen unit polyalanine oligomer CH_3–$CO(Ala)_{15}$–$NHCH_3$ are constructed using density-functional calculations for smaller model peptides. Energy levels as well as the transition dipoles of all singly and doubly excited-state manifolds are calculated. A variety of C_{13}-substituted isotopic derivatives are examined with respect to their ability to reveal differences in local secondary structures in two-dimensional infrared spectra in the amide I region. Amide mode anharmonicities are predicted to be valid indicators of secondary helical structures. © *2003 American Institute of Physics.* [DOI: 10.1063/1.1538243]

I. INTRODUCTION

Structural and dynamical properties of proteins determine their biological activities. A clear microscopic picture of protein folding facilitates the prediction of three-dimensional structures from primary sequences, a fundamental problem in molecular biology.[1–6] Experimental techniques including nuclear magnetic resonance (NMR),[7–9] linear optical, Raman, fluorescence,[10,11] small angle x-ray scattering,[12,13] and Laue diffraction[14,15] have been widely used to investigate proteins structures with nanosecond time resolution.

Vibrational (infrared and Raman) spectroscopy provides a direct probe for molecular structure. The localized nature of vibrational motions makes them a useful probe for secondary structures of proteins.[11,16] Various structural motifs such as α helices β sheets can often be clearly distinguished by changes in the linear infrared absorption.[17–21] The development of ~50 fs tunable infrared pulses had opened up the possibility of multidimensional coherent vibrational spectroscopy[24,25] which provides considerably more structural and dynamical information compared to linear (one-dimensional) spectroscopy, and could allow much more refined and specific structure determination. These techniques improve the spectral resolution in the same way as two-dimensional (2D) NMR[22,23] and offer the possibility of probing subpicosecond snapshots of protein structures.

In this work we predict specific signatures of local α- and 3_{10}-helical conformations for isotopomers of CH_3–$CO(Ala)_{15}$–$NHCH_3$ in linear and coherent nonlinear vibrational spectra. The primary differences between 3_{10} and α helices are the intramolecular hydrogen bonds which connect the $i-i+3$ and $i-i+4$ units, respectively. It was estimated that about 10% of helical structures in proteins adopt the 3_{10} conformation with a mean segment length of 3.3 units;[26] 3_{10} structure is generally found near the termini of polypeptide chains.[27,28] The 3_{10} helix was proposed as an intermediate in the folding of α helices,[27,29,30] a supposition that has been supported by molecular-dynamics simulations.[31–34] These studies predict a significant role of the 3_{10} conformation in protein dynamics. Identifying unique features of 3_{10} helices should allow the development of highly sensitive probes which could provide ultrafast snapshots of protein folding following a fast initiation (T jump, rapid mixing, or photochemical).[35–37]

Experimental evidence suggests that the relative stability of the α- and 3_{10}-helical conformations is solvent and peptide length dependent.[38–40] The α-helical content generally increases with peptide length and is further stabilized in aqueous solution.[40] Experimental electron spin polarization (ESR) studies show that polymers of less than 17 units primarily adopt the 3_{10} conformation. The 21mer exhibits both 3_{10} and α segments (α-helical in units 1–13).[38,39] NMR measurements also provide evidence of 3_{10} content in peptides with significant alanine composition,[27] pointing to structures that are about 50% and 25% 3_{10} at the termini and near the center of the oligomer, respectively. A positive correlation between α-helical composition and the water content of organic–aqueous solvent mixtures has been reported.[40]

Computational studies generally favor the α-helical conformation,[41–43] although a consensus has not been reached yet regarding the relative thermodynamic stability of the two conformations. A recent *ab initio* study predicts an increasing stability of the α-helix as the chain length is changed from 4 to 10 residues;[44] these calculations were done both *in vacuo* and in the presence of a dielectric continuum intended to simulate an aqueous environment. The 3_{10} conformation was the global minimum *in vacuo*, whereas the α-helix was found to be the global minimum in solution for molecules with at least 6 units. Two possible mechanisms for α to 3_{10} conversion were proposed which differ by the terminus where the conformational change is initiated at.

The amide I band (mostly the C═O stretch) of proteins may be adequately described by the eigenmodes in a basis of N local amide I coordinates (N is the number of carbonyl groups); these eigenmodes constitute vibrational

a)Electronic mail: mukamel@chem.rochester.edu

excitons.[45,46] The exciton formalism[17,47,48] provides a unified interpretive scheme for systems of arbitrary size and has been successfully applied to both linear[17,18,49] and nonlinear[50–55] optical measurements in the amide I bands of polypeptides.

Here we use DFT calculations for small segments (no more than 2 units) to parameterize model Hamiltonians of isotopic derivatives and identify linear and nonlinear spectroscopic signatures of local secondary structure. A similar strategy has been successfully employed in the construction of electronic exciton Hamiltonians for molecular aggregates.[56,57] Our results are not limited to polyalanine oligomers and should be transferable to other peptide systems. The *ab initio* parameterization of such a large system required a judicious mix of art and science, since there is no clear protocol for such a parameterization. Our objective was to select computationally tractable model systems that best approximated the force field of the entire molecule with respect to the modes of interest, the amide I and the amide A modes. The amide I mode possesses the characteristics needed for application of the exciton model; it is localized with a well defined internal coordinate composition.[17,58] Large changes in the reduced mass and distribution of amplitude do not occur in different conformers/secondary structures. The N–H stretch (amide A) is also highly localized with nearly all the amplitude in the N–H bond and therefore should also be amenable to this description. However, the physical interpretation of this band is complicated by a Fermi resonance of the NH stretch with the overtone of the amide II mode.[59] Nevertheless, a proper excitonic treatment of this mode should be attainable.

Excitonic Hamiltonians have been widely used in condensed matter physics to describe electronic excitations of extended systems composed of many similar repeat units, e.g., semiconductors, molecular crystals, and aggregates.[47,60] In periodic systems computational effort reduces to the size of the repeat unit; the physical size of the system is no longer a limitation. Exciton Hamiltonians were also constructed for vibrational motions in crystals[45] and proteins.[46] Peptides are not strictly periodic and a systematic first principles construction of an exciton Hamiltonian should address the issue of selecting natural repeat units and relevant modes; such a procedure is outlined below.

The exciton framework has been successfully employed in the simulation of linear infrared (IR) spectra for several globular protein segments.[17,18,49] Parameters of this model include transition frequencies and dipole derivatives of local amide I modes. The bilinear coupling coefficients between all pairs of local amide I modes were determined using an electrostatic transition dipole coupling (TDC) mechanism[58,61,62] previously used to parameterize the force field of both amide I and amide II modes in α-helices and β-sheets.[61,62] Advantages of such electrostatic mechanisms are obvious, making the coupling coefficients a simple function of the atomic coordinates. However, *ab initio* calculations suggest that this mechanism fails to predict the nearest-neighbor coupling of amide I modes,[50,63] meaning that through bond effects should not be neglected in this case.

The present work demonstrates the construction of a vibrational exciton Hamiltonian using quantum chemical *ab initio* methods and identifies 2D IR signatures of two well-defined structural motifs. In Sec. II we present the definition and parameterization of the local amide modes. The vibrational exciton Hamiltonian is described in Sec. III. The linear spectra of various isotopomers are described in Sec. IV, and Sec. V presents nonlinear infrared signatures (three pulse photon echoes). Our conclusions are given in Sec. VI.

II. THE LOCAL AMIDE MODES

Both α- and 3_{10}-helical structures were built using x-ray crystallographic data and ideal structural parameters. The experimental x-ray structure of the α helix was taken directly from Ref. 64. The 3_{10} structure was built using the ideal 3_{10} interunit torsion angles ($\phi=-49,\psi=-26$)[65] and crystallographic averages for all other coordinates.[66]

We start with the Hamiltonian for the local amide repeat units

$$H_0=\sum_{\alpha} H_{\alpha}(R), \tag{1}$$

where $\{\alpha\}$ denotes a repeat unit index and R represents internal coordinates (bond lengths and angles). The anharmonic vibrational Hamiltonian for the α repeat unit $[H_{\alpha}(R)]$ expanded to fourth order with respect to its internal coordinates is given by

$$H_{\alpha}(R)=V_0+\sum_i f_i R_i+\sum_i^N \frac{P_i^2}{2m_i}+\sum_{i,j}^N f_{ij}R_iR_j + \sum_{i,j,k}^N f_{ijk}R_iR_jR_k+\sum_{i,j,k,l}^N f_{ijkl}R_iR_jR_kR_l, \tag{2}$$

where the sums run over N internal coordinates and the nth order partial derivatives of the potential energy can be written as

$$f^{(n)}_{k1k2\ldots kn}=\frac{1}{n!}\left(\frac{\partial^n V}{\partial R_{k1}\partial R_{k2}\ldots\partial R_{kn}}\right)_0. \tag{3}$$

Five coordinates were included for each repeat unit: The C′═O, C′–N, and N–H stretches in addition to the C^{α}–C′–N and C′–N–H bending modes. The Hamiltonian parameters were computed at the DFT level. The GAUSSIAN 98 code was used for these and all other quantum chemical calculations.[67]

The α- and 3_{10}-helices possess three and two nonhydrogen bonded amide I modes on the nominal C-terminal end, respectively. The parameters of nonhydrogen-bonded modes at the ends of the helices were obtained using the anharmonic vibrational Hamiltonian of *trans*-N-methylacetamide (NMA), whereas calculations of the model alpha- and 3_{10}-helical NMA dimers shown in Figs. 1(c) and 1(d) were used for the remaining modes. The dimers were built using heavy atom coordinates taken directly from the α- and 3_{10}-helices. The internal coordinates within each member of the dimer were optimized at the three parameter Lee–Yang–Parr (B3LYP)/6-31+G** level, whereas all coordinates describing the relative orientation of the molecules and the

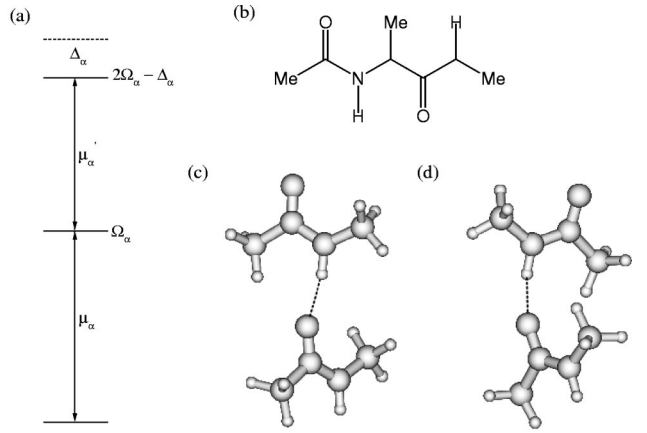

FIG. 1. (a) The three-level systems characterizing local amide modes (LAM) in the exciton Hamiltonian. The parameters Ω_α and Δ_α represent the fundamental transition energy and anharmonicity of mode *i*. The bilinear coupling between modes is represented by $J_{\alpha\beta}$. Transitions intensities are determined by the fundamental transition dipoles μ_α and μ'_α. (b) Model molecule used to calculate the amide I bilinear coupling between nearest neighbors. (c) and (d) NMA dimers $(CH_3CONHCH_3)_2$ used to parameterize amide I and amide A transition frequencies and couplings for the (c) α- and (d) 3_{10}-helices. Hydrogen bonds are represented by dashed lines.

N–O distance separating them were fixed. This procedure allowed the accurate calculation of force constants with minimal perturbation of the differences in interaction between hydrogen bonded neighbors of the two structures.

Anharmonic vibrational Hamiltonians [Eq. (2)] of the three model systems shown in Fig. 1 were constructed by calculating force constants of the C′═O, C′–N, and N–H stretches, C^α–C′–N, and C′–N–H to fourth order by numerically differentiating analytical second-order force constants obtained from Hessian calculations at the B3LYP/6-31+G** level. These coordinates were selected because they carry the most amplitude in the normal modes and when explicitly included in the Hamiltonian of NMA give a linear spectrum in which the relative intensities and frequencies differ by less than 20% from those obtained using a 3N-6 coordinate harmonic normal mode analysis.

We next transformed the quadratic part of Eq. (2) to obtain a set of normal modes Q_α. Out of these five modes found for each repeat unit we selected the two corresponding to the amide I and amide A normal modes. In terms of these *local amide modes* (LAM) we postulated the following form for the Hamiltonian:

$$H_0 = \tfrac{1}{2}\sum_\alpha (\Omega_\alpha - \Delta_\alpha)Q_\alpha^2 + \tfrac{1}{12}\sum_\alpha \Delta_\alpha Q_\alpha^4 - E(t)\sum_\alpha \mu_\alpha Q_\alpha, \quad (4)$$

where Ω_α, Δ_α, and μ_α are the frequency, anharmonicity and transition dipole of LAM α and $E(t)$ is the external optical field. We have diagonalized the anharmonic vibrational Hamiltonians $H_\alpha(R)$ by expanding it as a matrix in a harmonic basis and used the three lowest energy states in each LAM to obtain the parameters Ω_α and Δ_α which are presented in Table I.

TABLE I. DFT parameters of the exciton Hamiltonian of two helices.

Parameter[a]	α-helic	3_{10}-helix	NMA
Ω_I	1704.6	1701.4	1724.5
Ω_A	3365.2	3367.6	3467.9
Δ_I	14.8	14.8	17.1
Δ_A	52.9	45.4	24.8
θ_I	0.8°	2.8°	5.4°
θ_A	8.6°	11.5°	19.5°
$J^*_{I,I}$	10.0	4.5	⋯
$J_{I,I}$	−4.9	−5.9	⋯
$J_{I,A}$	−23.1	−29.15	⋯

[a]The symbols Ω and Δ represent fundamental transition energies and anharmonicities of the localized modes (in cm^{-1}). The angles θ_A and θ_I are the angles the transition dipole makes with respect to the N–H and C═O bonds for modes *A* and *I*, respectively. The amide I couplings between nearest and hydrogen bonded neighbors are denoted by $J^*_{I,I}$ and $J_{I,I}$, respectively.

Fermi resonance with the overtone of the amide II mode causes a splitting of the N–H fundamental into the amide A (3300 cm^{-1}) and amide B (3100 cm^{-1}) bands.[59] To test for the presence of Fermi resonances, transition frequencies of the N–H stretch were calculated for NMA using Hamiltonians with and without the other four coordinates. We found that the fundamental amide A transition energy increases by less than 1 cm^{-1} when the other four coordinates are included. A Fermi resonance is absent because the DFT calculation overestimates the amide A frequency to a larger degree than the amide II frequency. The experimental amide II and amide A fundamentals of gaseous NMA appear at 1510 and 3150 cm^{-1},[68] whereas 1566 and 3652 cm^{-1} are obtained using the B3LYP/6-31+G** level of theory. Furthermore, the frequency difference between the amide II and A modes decreases upon aqueous solvation,[68] whereas all DFT calculations were done in a vacuum. To recover the Fermi resonances it will be interesting to perform extensive *ab initio* calculations of small peptide–water clusters, since the site-specific hydrogen bonding interactions are not described by continuum models.

Finally, we turn to the transition dipole. In Eq. (4) we have expanded the dipole operator to first order in Q_α, and μ_α represents the dipole derivative with respect to the LAM α. Transition dipole orientations were taken from the calculations of the LAM for the model molecules shown in Fig. 1 and are presented in Table I. Calculations for isolated NMA were used to parameterize the transition dipole orientations of all non hydrogen bonded LAM, whereas those of the hydrogen bonded LAM were taken from the calculations for the NMA dimers. The angles for the local amide I and amide A modes denote the angle between the dipole derivative of the LAM with the C═O and N–H bonds, respectively. The amide I dipole derivative points to the nitrogen side of the C═O bond and the amide A points to the carbonyl side of the N–H bond. Both of these vectors reside in the O═CN plane.

The transition dipole magnitudes and positions of the amide I mode were taken from Refs. 17 and 63, respectively. The magnitudes were not taken from density-functional theory (DFT) calculations for the model molecules because

they were about a factor of 5 larger than those given in Ref. 17 (3.7 A $Å^{-1}$ amu^{-1}) and resulted in physically unreasonable bilinear coupling coefficients (see Sec. III A).

Defining the transition dipole magnitude of the N–H stretch is complicated by a Fermi resonance with the overtone of the amide II mode. However, it is sensible to estimate the local N–H dipole derivatives using the intensity of the amide A band for the following reasons: (i) Force fields constructed for polyalanine predict an intrinsic N–H stretching frequency (3314 cm^{-1})[59] which is nearly equivalent to the observed value (3311 cm^{-1}).[59] (ii) The integrated intensity of the amide A band comprises 80%–90% of the total intensity associated with the two N–H peaks.[69] The magnitude of the amide A transition dipole was taken to be 3/5 that of the amide I mode. This ratio is consistent with both the magnitudes of the calculated coupling coefficients and experimental extinction coefficients.[70]

III. THE VIBRATIONAL EXCITON HAMILTONIAN

The exciton Hamiltonian is finally obtained by introducing bilinear couplings $J_{\alpha\beta}$ between the LAM. We then write

$$H = H_0 + \sum_{\alpha<\beta} J_{\alpha\beta} Q_\alpha Q_\beta . \tag{5}$$

This Hamiltonian was expanded in a basis of all single and double excitations for the LAM. However, matrix elements between basis state manifolds with different numbers of excitations made negligible effects and were not included. Similar Hamiltonians were used in Refs. 52 and 71.

Equation (5) is based on the assumption that coupling between the local modes is dominated by the quadratic term; the cubic or quartic terms were neglected. This assumption is well justified for localized modes. Calculations for predominantly bond stretching modes of peptides presented here and for the carbonyl stretches of a rhodium complex[72] have shown that all mixed (multimode) third- and fourth-order coefficients in the expansion of the potential energy [Eq. (2)] are less than 5% the magnitude of the bilinear coefficients. It is, therefore, justified to treat sufficiently localized modes with an exciton model [Eq. (5)]. Diagonalization of the single exciton block of this Hamiltonian resembles a standard calculation of harmonic modes, whereas the double exciton block is diagonalized in a basis of direct product states of the local modes. The introduction of the anharmonicities Δ_α [Eq. (4)] is necessary for predicting nonlinear responses; the values of these parameters are supported by comparing our calculations to experiment.[53]

The origin of the bilinear coupling coefficients $J_{\alpha\beta}$ depends on the pair of LAM under consideration. The transition dipole coupling (TDC) model was used to calculate coupling coefficients between local amide I coordinates for nonnearest neighbors which are not connected with a hydrogen bond. Couplings between nearest neighbors were determined by calculating the off-diagonal second order energy derivative with respect to the two local amide I modes of the molecule shown in Fig. 1(b). All internal coordinates except ϕ and ψ, which were fixed to the ideal α- or 3_{10}-helical values, were optimized at the B3LYP/6-31+G** level prior to numerical differentiation. Similarly, amide I coupling coefficients between the modes of hydrogen bonded units were determined using the NMA dimers shown in Figs. 1(c) and 1(d).

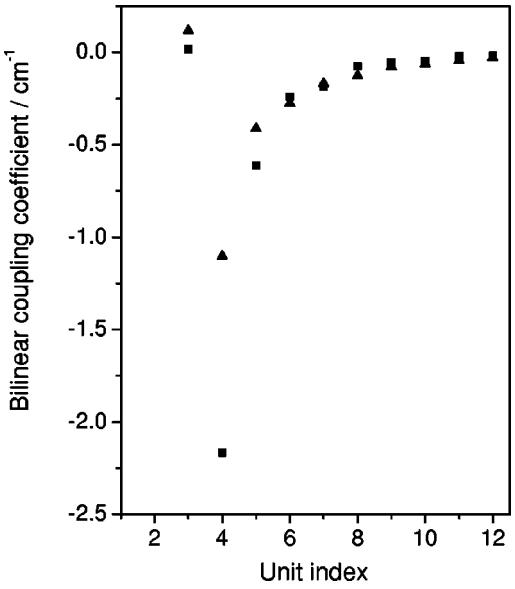

FIG. 2. Bilinear coupling coefficients of the α- (squares) and 3_{10}- (triangles) helices taken directly from the off-diagonal N–H force constants of an AM1 Hessian calculation. The coefficients correspond to the nominal N-terminus N–H and the unit index indicated on the abscissa ($J_{1\beta}$).

Coupling coefficients between amide A modes (see Fig. 2) were taken directly from the force constant output of a semiempirical AM1 Hessian calculation; these are about a factor of 3 smaller than the amide I coefficients (the maximum is <3.0 cm^{-1}). Interestingly, the signs and magnitudes of the force constants between N–H coordinates show the same pattern as the TDC coupling coefficients of the amide I for both the α[17] and 3_{10} helices, suggesting the coupling coefficients between amide A modes possess TDC character.

Bilinear couplings between amide I and amide A modes were obtained by numerical differentiation for coordinates belonging to the same amide group (O═C′–N–H) (using NMA) (-12.6 cm^{-1}) and for hydrogen bonded neighbors [using the NMA dimers, Figs. 1(c) and 1(d)]. The coupling elements between all other pairs of modes are negligible (<1 cm^{-1}) relative to their frequency differences (>1500 cm^{-1}) and therefore were not included in the Hamiltonian.

IV. INFRARED ABSORPTION OF α- AND 3_{10} HELICES

Figure 3 shows the linear spectra of the α- and 3_{10}-helices for the unsubstituted (^{12}C) compounds in both the amide I and amide A regions. Note that the calculated frequencies are overestimated by about 50 cm^{-1} compared to experiment.[18] However, it is the relative (not the absolute) frequencies that are most important here. The primary difference between these spectra is an overall redshift (10 cm^{-1}) of the amide I transitions for the 3_{10}-helix, although this may be difficult to observe in nature where disorder and short 3_{10} structure prevail. For this reason, we turned to isotopic derivatives to reveal the local structure.

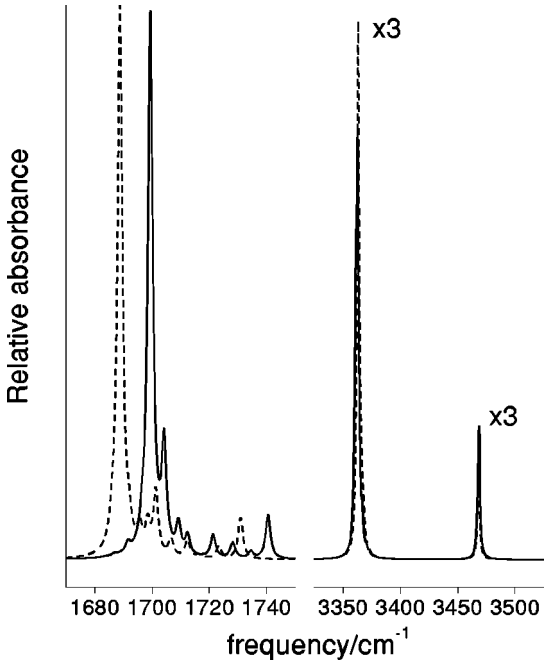

FIG. 3. Linear infrared spectra of unsubstituted (^{12}C) CH_3–$CO(Ala)_{15}$–$NHCH_3$ for the α- (solid) and 3_{10}- (dashed) helices in the (a) amide I and (b) amide A regions.

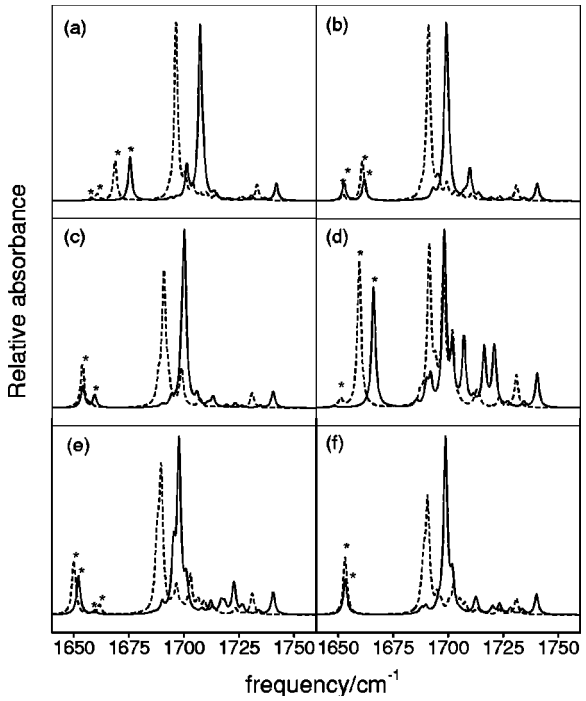

FIG. 4. Linear infrared spectra of α- (solid) and 3_{10}- (dashed) isotopomers with ^{13}C labels on various units (a) 1 and 2, (b) 1 and 3, (c) 1 and 4, (d) 7 and 8, (e) 7 and 9, (f) 7 and 10. Peaks corresponding to modes localized on the isotopically substituted units are labeled with asterisks.

Hamiltonians of eight isotopic derivatives were generated. Frequencies of isotopically substituted local modes were reduced by 43.5 cm^{-1} based on the calculated shift for NMA at the B3LYP/6-31+G** level, which is consistent with experimental measurements.[52] Hamiltonians with isotopic substitutions in the middle and on the nominal N-terminal end of chains were calculated. Isotopic derivatives are not needed to deduce secondary structure on the C-terminal end because these units are naturally decoupled due to the absence of intramolecular hydrogen bonds; the α-helix exhibits a higher frequency band because it possesses three non hydrogen bonded carbonyls at the end as opposed to only two in the 3_{10}-helix.

Linear spectra of the six isotopomers formed by making two ^{13}C substitutions for carbonyl carbons (a) 1 and 2 (b) 1 and 3 (c) 1 and 4 (d) 7 and 8 (e) 7 and 9 (f) 7 and 10 are shown in Fig. 4 (the indices run from the nominal N-terminus to the C-terminus). The Lorentzian linewidth of all transitions was set to 2 cm^{-1} (fwhm). Differences in the splitting and relative intensities of the two lowest frequency peaks (labeled with asterisks) are apparent between the two conformations. Isotopic labels on nearest neighbors reveal greater bilinear coupling for the α-helix; the energy gaps between the two lowest energy transitions for the α and 3_{10} conformers are 8.8 and 19 cm^{-1} for the 1,2 substituted molecule and 8.5 and 18 cm^{-1} for the 7,8 isotopomer, respectively. The 1,3 and 7,9 units couple more strongly in the 3_{10}-helix due to hydrogen bond connectivity, which is especially evident in the peak splitting of the 7,9 isotopomer (α=7.3 cm^{-1}, 3_{10}=11.6 4.5 cm^{-1}). The 1,4 carbonyl groups couple through an intramolecular hydrogen bond in the α-helix, which results in a pair of transitions with a distinctly different intensity ratio from that of the 3_{10}-helix. The 7,10 isotopomers of both helices couple to give a strong and an extremely weak peak, so the relative splitting is not seen for this isotopomer. The differences predicted for these bisubstituted isotopomers are relatively subtle. It is therefore sensible to investigate the effects of substituting three and four ^{13}C in a sequence to attain a more robust distinction.

Linear spectra of isotopomers formed by replacing both three and four carbonyl carbons with ^{13}C isotopes are presented in Fig. 5. Substitutions were introduced for units (a) 1, 2, and 3 (b) 7, 8, and 9 (c) 1, 2, 3, and 4 (d) 7, 8, 9, and 10. The peaks which represent modes localized on the isotopically substituted units are labeled with asterisks. As with the bisubstituted compounds, differences in intensity and frequency splitting are immediately obvious and are as easily interpreted here. Both the 1-2-3 and 7-8-9 isotopomers yield a strong peak along with two relatively weak peaks for both helices and are, therefore, not optimal choices for investigating local structure. The 1-2-3-4 isotopomers give multiple strong peaks for the 3_{10}- but not the α-helix where a single strong peak is calculated. The same is seen for the 7-8-9-10 isotopomers. Such features should be easily distinguishable by infrared (IR) measurements. Although it is not evident by examining Figs. 5(c) and 5(d), the peaks appearing at about 1670 cm^{-1} for the α-helix are actually composed of two nearly degenerate transitions. These transitions are calculated at 1670.9 and 1671.0 cm^{-1} (transition dipoles are 4.4 and 7.3 D) for the 1–4 isotopomer and at 1668.3 and 1669.1 cm^{-1} (transition dipoles are 1.6 and 9.5 D) for the 7–10 isotopomers. These derivatives are, therefore, the optimal choices for probing local secondary structure in the two helices.

Obtaining a localized picture for the amide A mode is

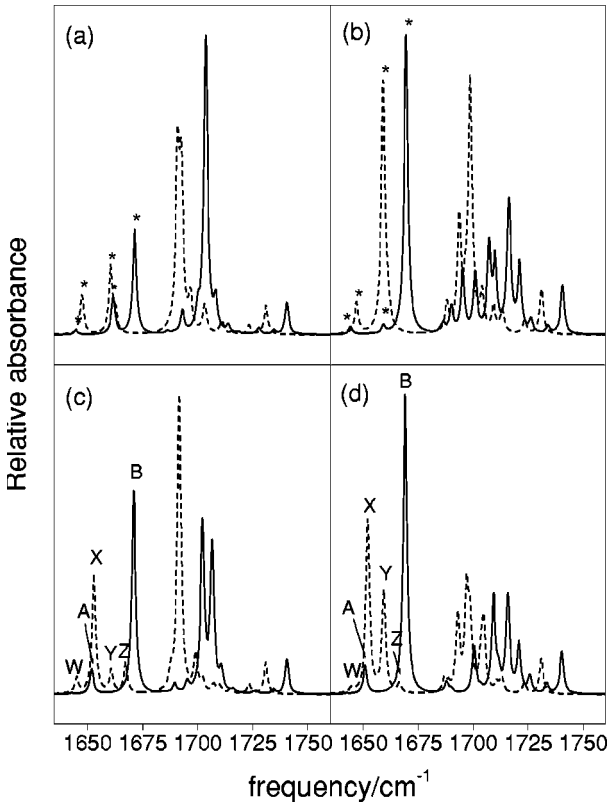

FIG. 5. Linear infrared spectra of the α- (solid) and 3_{10}- (dashed) isotopomers with ^{13}C labels on the units (a) 1, 2, and 3 (b) 7, 8, and 9 (c) 1, 2, 3, and 4 (d) 7, 8, 9, and 10. Peaks corresponding to modes localized on the isotopically substituted units are labeled with asterisks in panels a-b and with letters (A-B, W-Z) in panels (c) and (d).

less straightforward than for amide I; isotopic substitutions of ^{15}N is predicted to decrease the vibrational frequency by only 6 cm^{-1} (B3LYP/6-31+G** calculation for NMA) and deuteration of this group is complicated by migration of the isotopic label. However, our calculations predict that the anharmonicity of this mode in the α-helix is 7.5 cm^{-1} greater than that of the 3_{10} (Table I). While this signature is not as robust as for the isotopomers in the amide I region, it is within experimental resolution and could easily be verified by nonlinear measurements of prototypical α and 3_{10}-oligomers.

V. NONLINEAR IR SIGNATURES OF α- AND 3_{10}-HELICES

Although the calculated linear peak positions and intensities can distinguish local secondary structures, the picture may not be so clear experimentally since line broadening usually limits the resolution and eliminates many fine details. Multidimensional infrared techniques carry more information and should therefore be applied in ambiguous cases, as is commonly done in NMR[22] and ESR.[73] Predictions of qualitative relations between the resonances are more practical tools for interpretation because multidimensional nonlinear spectra possess more features. The most accessible difference between the two helices is the occurrence of nearly degenerate transitions in the 1-2-3-4 and 7-8-9-10 isotopomers for the α-helix but not the 3_{10}-helix. These transitions are spectrally unresolvable (separated by 2 cm^{-1}). However, these features are easily seen in the Wigner spectrogram of the signal.[74–76]

Figure 6 shows the absolute value of the two-pulse photon echo (PE) signal for the 1-2-3-4 and 7-8-9-10 isotopomers plotted in the frequency domain,[48] where the spectral region corresponding to only the vibrations localized on the isotopically labeled units is displayed. For a precise definition of these plots see Ref. 77: The peaks in the PE spectrum represent vibrational coherences during the first and third time intervals in the incident pulse sequence. The second time interval was zero and the homogeneous dephasing constant Γ was set equal to 1 cm^{-1}. The incident pulse widths span the entire amide I region of the spectrum and possess uniform intensity (rectangular shape in the frequency domain) for this spectral region. The rotating wave approximation was applied manually by selecting the relevant Liouville space pathways and the pulses were taken to be impulsive in the time domain (the snapshot limit).[48] The polarizations of all four fields were parallel and the signals were averaged over molecular orientations.[78]

Peaks representing the vibrational fundamentals appear on the diagonal axis ($\omega_1=\omega_3$) of Fig. 6. The peak labels correspond to the indices assigned in Figs. 5(c) and 5(d) and represent the coherence frequencies during the first and third time intervals. For example, the peak labeled X,X in panel (a) evolves at 1652 cm^{-1} during both the first and third time intervals. A peak corresponding to the singly to doubly excited state transition is seen shifted down the ω_3 axis from the corresponding fundamental by the anharmonicity. For example, the peak labeled X,XX in panel (a) evolves at 1652 and 1643 cm^{-1} during the first and third time intervals, respectively. Thus the anharmonicity of mode X is 9 cm^{-1}. The best resolved peaks are seen for the strongest transitions in the linear spectra as the PE response function is fourth order in the transition dipole, making the display of all peaks on the same scale problematic. The anharmonicity for the overtone of the strongest IR active mode is labeled for each conformer in Fig. 6.

Cross peaks between different modes appear at frequencies corresponding to the two fundamentals. For example, the peak labeled "X,Z" in panel (a) evolves at 1652 and 1667 cm^{-1} during the first and third time intervals, respectively. The combination bands between these modes are shifted down the ω_3 axis by an amount equal to the anharmonicity of the combination band. For example, the peak labeled X,XZ is shifted down the ω_3 axis from the peak X,Z by 7 cm^{-1}, the anharmonicity of this combination band.

Note that the anharmonicities of the singly to doubly excited state transitions for isotopically labeled modes in the α-helix (4–6 cm^{-1}) are significantly smaller than in the 3_{10} (10–12 cm^{-1}), a difference that may be easily resolved experimentally. This result is robust because it represents local secondary structure rather than the energy levels of the entire 15 unit ideal helices, which of course do not exist in solution.

The frequency domain is not the only way to view this measurement; the relative anharmonicities may also be revealed as beat frequencies at certain spectral regions in the radiated field. A 2D IR signal that carries more information is

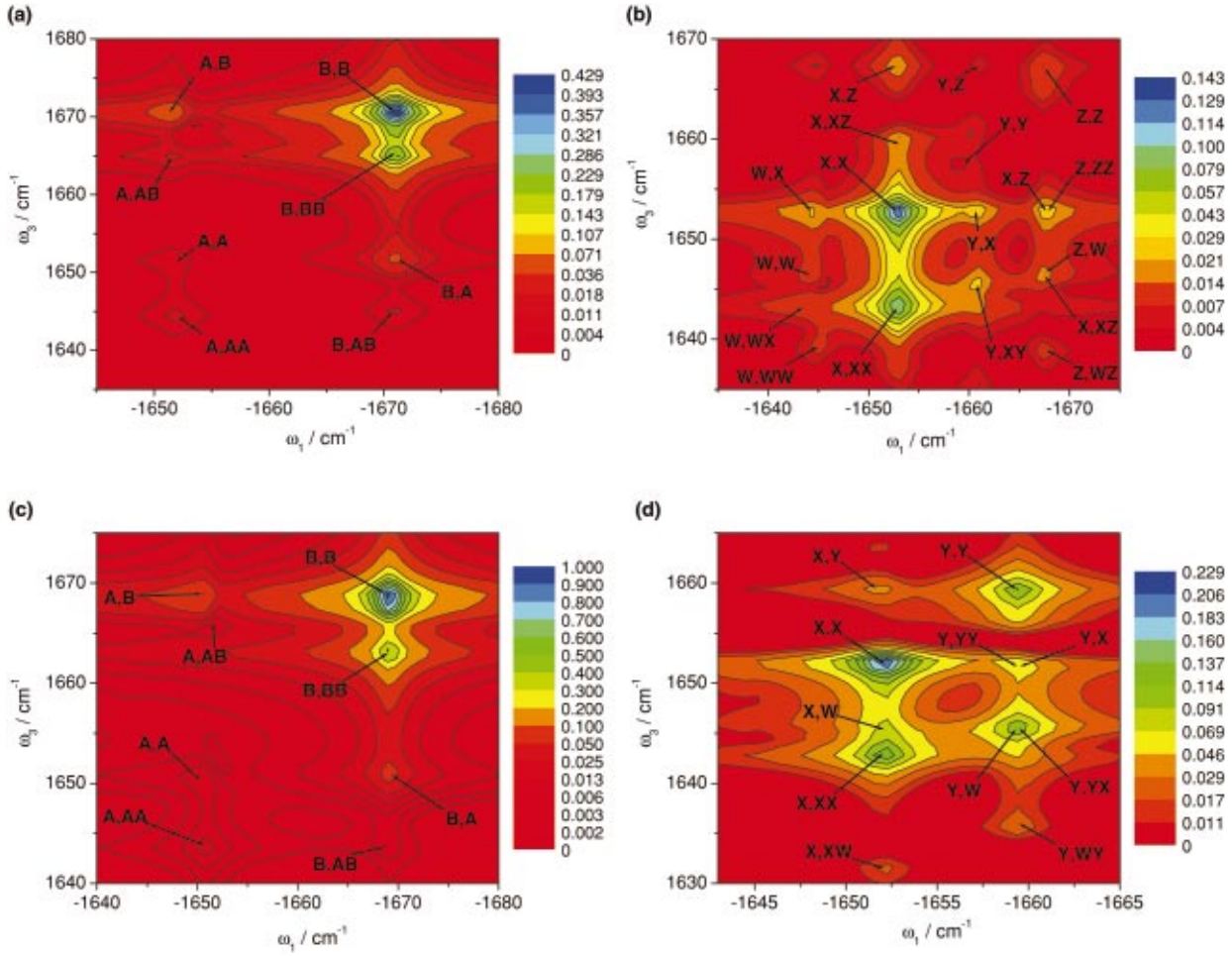

FIG. 6. (Color) Absolute value of the three pulse IR photon echo spectra of the 1-2-3-4 substituted (a) α- and (b) 3_{10}-isotopomers are shown along with the 7-8-9-10 substituted (c) α- and (d) 3_{10}-isotopomers. Axes correspond to the Fourier transform with respect to the third time interval. The second time interval is set to $t_2=0$. The peak labels correspond to the indices assigned in Figs. 5(c) and 5(d). All four field polarizations were taken to be parallel and the spectra have been normalized to the maximum intensity for the 7-8-9-10 α-helix.

the Wigner spectrogram, which is bilinear in the response function R and is defined by the transformation

$$S_{ijkl}(\omega_3;t_3,t_2,t_1)=\int d\tau R_{ijkl}(t_3+\tau/2,t_2,t_1) \times R^*_{ijkl}(t_3-\tau/2,t_2,t_1)\exp(i\omega_3\tau), \tag{6}$$

where the indices *ijkl* represent the lab frame polarizations of the four fields. The spectrogram represents the joint time (t_3) and frequency (ω_3) distribution of the emitted field. Peaks appear at frequencies corresponding to the average of all pairs of resonances seen in the frequency domain spectra along ω_3 (see Fig. 6). All peaks in the spectrogram are modulated at the frequency difference between the respective resonances.

The smaller anharmonicities of the α-helix are evident in the Wigner spectrograms displayed in Fig. 7; these spectrograms correspond to the PE spectra shown in Fig. 6. The peaks appearing at the average of the fundamental and overtone frequencies ($\alpha\approx1667$ cm^{-1}, $3_{10}\approx1647$ cm^{-1}) are clearly modulated at lower frequencies for the α-helix (period ≈5 ps) than for the 3_{10}-helix (period ≈3.3 ps).

VI. CONCLUSIONS

Our results for this simple peptide exemplify subtle differences in the vibrational spectra of closely related structures. We have demonstrated that *ab initio* calculations of small model systems can be used to parameterize high-quality spectroscopic Hamiltonians, facilitating a detailed interpretation of nonlinear signals and resolution of ambiguous linear measurements. The exciton description was applied to the amide I and amide A modes. Linear and nonlinear IR signatures of local α- and 3_{10}-helical structure for a series of C_{13}-substituted isotopomers were identified. Local secondary structure is manifested in the peak positions and intensities of the linear spectra for the 1-2-3-4 and 7-8-9-10 C_{13}-substituted isotopomers. In addition, nonlinear PE signals were both plotted in the frequency domain and as Wigner spectrograms to reveal the relative magnitudes of the overtone anharmonicities calculated for the two structures. The anharmonicities of the overtone transitions in the 3_{10}-helix (10–12 cm^{-1}) were calculated to be about twice those of the α-helix (4–6 cm^{-1}). It will be interesting to explore other structural motifs such as β-sheets in the future.

Even though the calculations presented here should be

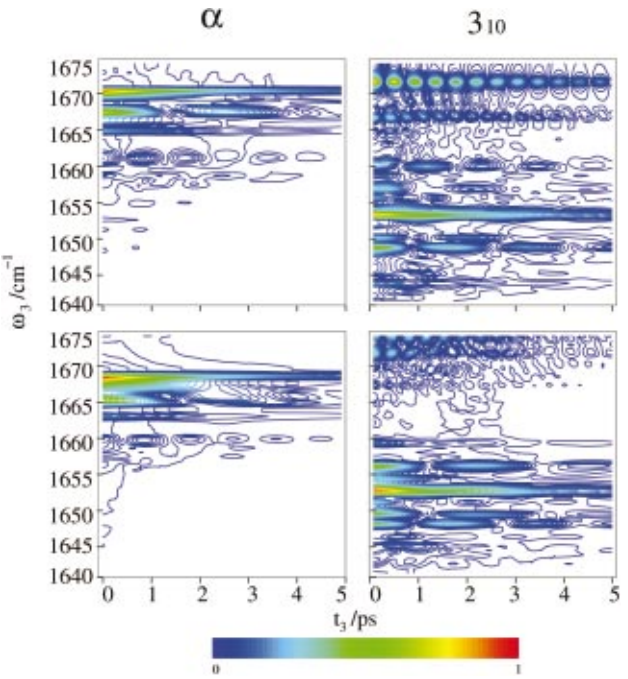

FIG. 7. (Color) The Wigner spectrogram $|S_{ZZZZ}(\omega_3;t_3,t_2,t_1)|$ of the nonlinear IR photon echo spectra shown in Fig. 6 for the 1-2-3-4 substituted (a) 3_{10}- and (b) α-isotopomers are shown along with the 7-8-9-10 substituted (c) 3_{10}- and (d) α-isotopomers. All spectra have been normalized to the maximum intensity for the 7-8-9-10 α-helix.

sufficient to characterize the local α- and 3_{10}-helical structures of polyalanine oligomers, it is worthwhile to note some of the difficulties encountered during the course of this work. Attempts to apply this formalism to the amide II mode were complicated by delocalization of the vibrational amplitudes; making the composition of this mode highly sensitive to the local conformation. Thus, parameters calculated for smaller systems may not be generally transferable to larger structures. Rather than forcing a description on amide modes of native peptides, a more viable approach will be to probe vibrational modes localized on side chains; synthetic derivatives can be used to label side chains with substituents that possess spectrally isolated and spatially localized modes. This strategy is particularly attractive since such modes do not form delocalized bands, making the interpretation of polarized measurements more viable.

ACKNOWLEDGMENTS

The support of NIH Grant No. GM59230-01A2 and NSF Grant No. CHE-0132571 is gratefully acknowledged. J.D. would like to thank the Max-Kade foundation for financial support of his stay in Rochester.

[1] M. Karplus and E. Shakhnovich, in *Protein Folding*, edited by T. Creighton (W. H. Freeman and Company, New York, 1992), pp. 127–195.
[2] C. Dobson, A. Sali, and M. Karplus, Angew. Chem. Int. Ed. Engl. **37**, 868 (1998).
[3] *Reaction Path Studies of Biological Molecules*, edited by R. Elber (World Scientific, Singapore, 1996).
[4] Y. Duan and P. Kollman, Science **282**, 740 (1998).
[5] N. Socci, J. Onuchic, and P. Wolynes, J. Chem. Phys. **104**, 5860 (1996).
[6] N. Socci, J. Onuchic, and P. Wolynes, Proteins: Struct., Funct., Genet. **32**, 136 (1998).
[7] J. Balbach, J. Am. Chem. Soc. **122**, 5887 (2000).
[8] T. Kuhn and H. Schwalbe, J. Am. Chem. Soc. **122**, 6169 (2000).
[9] M. Pfuhl and P. Driscoll, Philos. Trans. R. Soc. London, Ser. A **358**, 513 (2000).
[10] X. Chen, P. Li, J. Holtz, Z. Chi, V. Pajcini, and A. Asher, J. Am. Chem. Soc. **118**, 9705 (1996).
[11] *Biological Applications of Raman Spectroscopy*, edited by T. Spiro (Wiley-Interscience, New York, 1987), Vol. I.
[12] D. Segel, A. Bachman, J. Hofrichter, K. Hodgson, S. Doniach, and T. Kiefhaber, J. Mol. Biol. **288**, 489 (1999).
[13] S. Arai and M. Hirai, Biophys. J. **76**, 2192 (1999).
[14] B. Perman, S. Anderson, M. Schmidt, and K. Moffat, Cell Mol. Biol. (Paris) **46**, 895 (2000).
[15] T. Hori, H. Moriyama, J. Kawaguchi, Y. Hayashi-Iwasaki, T. Oshima, and N. Tanaka, Protein Eng. **13**, 527 (2000).
[16] *Infrared Spectroscopy of Biomolecules*, edited by H. Mantsch and D. Chapman (Wiley-Liss, New York, 1996).
[17] H. Torii and M. Tasumi, J. Chem. Phys. **96**, 3379 (1992).
[18] H. Torii and M. Tasumi, in *Infrared Spectroscopy of Biomolecules*, edited by H. Mantsch and D. Chapman (Wiley-Liss, New York, 1996).
[19] D. Byler and H. Susi, Biopolymers **25**, 469 (1986).
[20] W. Surewicz and H. Mantsch, Biochim. Biophys. Acta **952**, 115 (1988).
[21] M. Jackson, P. Haris, and D. Chapman, J. Mol. Struct. **214**, 329 (1989).
[22] R. Ernst, G. Bodenhausen, and A. Wokaun, *Principles of Nuclear Magnetic Resonance in One and Two Dimensions* (Clarendon, Oxford, 1987).
[23] K. Wütrich, *NMR of Proteins and Nucleic Acids* (Wiley, New York, 1995).
[24] Y. Tanimura and S. Mukamel, J. Chem. Phys. **99**, 9496 (1993).
[25] S. Mukamel and R. Hochstrasser, eds., *Special Issue on Chem. Phys. on Multidimensional Spectroscopy*, Vol. 266 (2001).
[26] D. Barlow and J. Thornton, J. Mol. Biol. **201**, 601 (1988).
[27] G. Millhauser, C. Stenland, P. Hanson, K. Bolin, and J. v. v. V. Frank, J. Mol. Biol. **267**, 963 (1997).
[28] J. Richardson and D. Richardson, *Predictions of Protein Structure and the Principles of Protein Conformation* (Plenum, New York, 1989).
[29] G. Millhauser, Biochemistry **34**, 3874 (1995).
[30] H. Long and R. Tycko, J. Am. Chem. Soc. **120**, 7039 (1998).
[31] J. Tirada-Rives and W. Jorgensen, Biochemistry **34**, 3864 (1991).
[32] K. Soman, A. Karimi, and D. Case, Biochemistry **31**, 1351 (1991).
[33] D. Tobias and C. Brooks, Biochemistry **30**, 7614 (1991).
[34] W. Young and C. Brooks, J. Mol. Biol. **259**, 560 (1996).
[35] P. Thompson, W. Eaton, and J. Hofrichter, Biochemistry **36**, 9200 (1997).
[36] Protein folding Special Issue, edited by J. S. Valentine, Acc. Chem. Res. **31**, 697 (1998).
[37] M. Grubele, J. Sabelko, R. Ballew, and J. Ervin, Acc. Chem. Res. **31**, 699 (1998).
[38] S. Miick, G. Martinez, W. Fiori, A. Todd, and G. Millhauser, Nature (London) **359**, 653 (1992).
[39] P. Hanson, D. Anderson, G. Mertinez, G. Millhauser, F. Formaggio, M. Crisma, C. Toniolo, and C. Vita, Mol. Phys. **95**, 957 (1998).
[40] T. Yokum, T. Gauthier, R. Hammer, and M. McLaughlin, J. Am. Chem. Soc. **119**, 1167 (1997).
[41] L. Zhang and J. Hermans, J. Am. Chem. Soc. **116**, 11915 (1994).
[42] M. Smythe, S. Huston, and G. Marshall, J. Am. Chem. Soc. **115**, 11594 (1993).
[43] J. Tirada-Rives, D. Maxwell, and W. Jorgensen, J. Am. Chem. Soc. **115**, 11590 (1993).
[44] I. Topol, K. Stanley, E. Deretey, T. Ting-Hua, A. Perczel, A. Rashin, and I. Czismadia, J. Am. Chem. Soc. **123**, 6054 (2001).
[45] R. Kopelman, in *Excited States*, edited by E. C. Lim (Academic, New York, 1975), Vol. 2.
[46] A. C. Scott, Phys. Rep. **217**, 1 (1992).
[47] V. Capek and E. Silinsh, *Organic Molecular Crystals: Interaction, Localization, and Transport Phenomena* (AIP, New York, 1994).
[48] S. Mukamel, *Principles of Nonlinear Optical Spectroscopy* (Oxford University Press, New York, Oxford, 1995).
[49] H. Torii and M. Tasumi, J. Chem. Phys. **97**, 92 (1992).
[50] P. Hamm, W. DeGrado, and R. Hochstrasser, Proc. Natl. Acad. Sci. U.S.A. **96**, 2036 (1999).
[51] S. Woutersen and P. Hamm, J. Phys. Chem. B **104**, 11316 (2000).
[52] S. Woutersen and P. Hamm, J. Chem. Phys. **114**, 2727 (2001).
[53] P. Hamm, H. Lim, and R. Hochstrasser, J. Phys. Chem. B **102**, 6123 (1998).
[54] A. Piratinski, S. Tretiak, V. Chernyak, and S. Mukamel, J. Raman Spectrosc. **31**, 125 (2000).

[55] S. Woutersen, Y. Mu, G. Stock, and P. Hamm, Proc. Natl. Acad. Sci. U.S.A. **98**, 11254 (2001).
[56] S. Tretiak, W.-M. Zhang, V. Chernyak, and S. Mukamel, Proc. Natl. Acad. Sci. U.S.A. **96**, 13003 (1999).
[57] T. Minami, S. Tretiak, V. Chernyak, and S. Mukamel, J. Lumin. **87–89**, 115 (1999).
[58] S. Krimm and J. Bandekar, Adv. Protein Chem. **38**, 181 (1986).
[59] S. Lee, N. Mirkin, and S. Krimm, Biopolymers **49**, 195 (1989).
[60] A. Davydov, *Theory of Molecular Excitons* (Plenum, New York, 1971).
[61] S. Krimm and Y. Abe, Proc. Natl. Acad. Sci. U.S.A. **69**, 2788 (1972).
[62] W. Moore and S. Krimm, Proc. Natl. Acad. Sci. U.S.A. **72**, 4933 (1975).
[63] H. Torii and M. Tasumi, J. Raman Spectrosc. **29**, 81 (1998).
[64] S. Arnott and A. Wonacott, J. Mol. Biol. **21**, 371 (1966).
[65] T. Creighton, *Proteins: Structures and Molecular Properties* (W. H. Freeman, New York, 1993).
[66] R. Engh and R. Huber, Acta Crystallogr., Sect. A: Found. Crystallogr. **47**, 392 (1991).
[67] M. J. Frisch, G. W. Trucks, H. B. Schlegel *et al.*, GAUSSIAN 98, Rev. A.9, Gaussian, Inc., Pittsburgh, PA (1998).
[68] N. Mirkin and S. Krimm, J. Am. Chem. Soc. **113**, 9742 (1991).
[69] E. Brazhnikov and Y. Chirgadze, J. Mol. Biol. **122**, 127 (1978).
[70] B. Lal and L. Nafie, Biopolymers **21**, 2161 (1982).
[71] C. Scheurer, A. Piryatinski, and S. Mukamel, J. Am. Chem. Soc. **123**, 3114 (2001).
[72] A. Moran, J. Dreyer, and S. Mukamel, J. Chem. Phys. **118**, 1347 (2003).
[73] J. Freed, Annu. Rev. Phys. Chem. **51**, 655 (2000).
[74] T. Meier, V. Chernyak, and S. Mukamel, J. Chem. Phys. **107**, 8759 (1997).
[75] S. Mukamel, J. Chem. Phys. **107**, 4165 (1997).
[76] W. Zhang, V. Chernyak, and S. Mukamel, J. Chem. Phys. **108**, 7763 (1998).
[77] A. Piryatinsky, V. Chernyak, and S. Mukamel, Chem. Phys. **266**, 285 (2001).
[78] R. M. Hochstrasser, Chem. Phys. **266**, 273 (2001).